

# Solenoid-free current drive via ECRH in EXL-50 spherical torus plasmas

Yuejiang Shi\*, Bing Liu\*, Shaodong Song, Yongyang Song, Xianming Song, Bowei Tong, Shikui Cheng, Wenjun Liu, Mingyuan Wang, Tiantian Sun, Dong Guo, Songjian Li, Yingying Li, Bin Chen, Xiang Gu, Jianqing Cai, Di Luo, Debabrata Banerjee, Xin Zhao, Yuanming Yang, Wenwu Luo, Peihai Zhou, Yu Wang, A.Ishida, T. Maekawa, Minsheng Liu, Baoshan Yuan, Y-K Martin Peng\* and the EXL-50 team

Hebei Key Laboratory of Compact Fusion, Langfang 065001, China

Enn Science and Technology Development Co., Ltd, Langfang 065001, China

\*E-mail of corresponding author: [shiyuejiang@enn.cn](mailto:shiyuejiang@enn.cn) [liubingw@enn.cn](mailto:liubingw@enn.cn) [pengyuankai@enn.cn](mailto:pengyuankai@enn.cn)

## Abstract

As a new spherical tokamak (ST) designed to simplify engineering requirements of a possible future fusion power source, the EXL-50 experiment features a low aspect ratio (A) vacuum vessel (VV), encircling a central post assembly containing the toroidal field coil conductors. Multiple electron cyclotron resonance heating (ECRH) resonances are located within the VV to improve current drive effectiveness. Copious energetic electrons are observed via hard X-ray detectors, carry the bulk of the plasma current ranging from 50kA to 150kA, which is maintained for more than 1s duration. It is observed that over one Ampere current can be maintained per Watt of ECRH power issued from the 28-GHz gyrotrons. The plasma current with high line-density (approaching  $10^{19}\text{m}^{-2}$ ) has been achieved for plasma currents as high as 76kA. An analysis was carried out combining reconstructed multi-fluid equilibrium, guiding-center orbits, and resonant heating mechanisms. It is verified that in EXL-50 a broadly distributed current of energetic electrons creates smaller closed magnetic-flux surfaces of low aspect ratio that in turn confine the thermal plasma electrons and ions and participate in maintaining the equilibrium force-balance.

**Spherical torus and Solenoid-free current drive.** Great progress has been achieved in magnetic confinement fusion research based on the Tokamak since 50 years ago when the first stable high temperature plasma was observed in the T-3 tokamak [1,2]. The tokamak has been the most investigated and furthest advanced configuration among the magnetic confinement fusion systems. More recently, the spherical torus (ST) concept of aspect ratios around 1.5 [3, 4] has been experimentally (START [5], NSTX [6], MAST [7], and Globus-M [8]) tested to realize a substantially higher plasma beta compared to the tokamak of aspect ratios around 3, and is an attractive candidate for realizing a relatively compact fusion reactor.

The tokamak plasma current is required to insure a high plasma confinement capability to restrain transport losses from the core to the edge. The start-up and ramp-up of this current has been commonly driven by a toroidal electric field induced by current changes in a centre solenoid (CS) magnet. This however causes engineering difficulties for the ST due to the limited space available within a narrow centre column. Further, a CS magnet is capable of sustaining the plasma current over limited time periods, which is to be augmented by non-inductive methods in a future fusion reactor. To develop a solenoid-free current drive capability therefore has been an important research endeavour for the STs. On the positive side, removing the CS allows additional space to increase the toroidal field (TF), further improving compactness and economy.

The original physics concept and principle of the ENN Spherical Torus with a major radius 58 cm (EXL-50) in Energy iNNovation (ENN) Science and Technology Development Co. was recently proposed by Peng [9]. One of the key EXL-50 experimental goals is to test the effectiveness of electron cyclotron resonance heating (ECRH) and current drive in the absence of an CS magnet. CS-free ECRH and current drive has been tested in several earlier ST devices (CDX-U [10], LATE [11-15], TST-2 [16-17], MAST [18-19], and QUEST [20-26]). A toroidal current of 1.05 kA was generated using about 8 kW of ECRH power on CDX-U [9], proving the possibility of current start-up by ECRH alone. Later, a 7kA plasma current was generated by about 30kW ECRH in LATE [11-12]. A current flattop with closed flux surface (CFS) plasma was sustained for 60ms in LATE, proving the potential for steady-state ECRH and current drive of the ST plasmas. In MAST, a plasma current of 73kA was produced by 60kW ECRH power with the help of the unique grooved mirror-polarizer installed on the central rod [18]. In QUEST, a plasma current of 90kA

was obtained with about 200kW ECRH power through combined first and second harmonic resonances [24].

In this paper, we present the latest ECRH experimental results from EXL-50. Not only are the operational parameters of CS-free current drive by ECRH significantly expanded, but also observed are some remarkable plasma behaviour. Discharges with plasma currents substantially above 100kA are routinely obtained in EXL-50, with the current flat-top sustained for up to or beyond 2 seconds. More than 1A current per Watt of ECRH power issued from the gyrotrons, averaged over hundreds of discharges, have been accumulated. At line-densities approaching  $10^{19}\text{m}^{-2}$ , plasma currents as high as 76kA have been achieved.

**The EXL-50 device is a medium-sized ST with a cylindrical vacuum vessel** (see, Fig. 1). Six poloidal field (PF) coils are located outside the vacuum vessel and the TF coil conductors. Inner limiters on the center column and outer limiters on the vessel wall have leading edges at 0.186m and 1.512m in major radius, respectively. The design of large space of EXL-50's vessel is mainly for the confinement and accommodation of energetic electrons whose spatial distribution area is larger than that of thermal plasmas. Two microwave frequencies have been utilized so far, 28-GHz from high power gyrotrons for higher toroidal field discharges and 2.45-GHz from low power magnetrons for lower toroidal field discharges and wall cleaning. Fig.1 shows the poloidal cross section of the EXL-50 device. Two sets of 28GHz gyrotrons (50kW source power for ECRH1 and 400kW for ECRH2) are available to inject power through an outboard ports above the mid-plane. Another 400kW 28GHz gyrotron (ECRH3) and two sets of 2.45GHz magnetrons (30kW source power each) are available to inject power through the mid-plane ports. The toroidal injection angles of the ECRH systems can be adjusted over limited ranges (as shown in Fig.1b). Both the 2.45-GHz and the 28-GHz systems are arranged to inject primarily ordinary-mode (O-mode) wave in recent experiments on the EXL-50. When the electric current of a 12-turn TF coils per turn was set to about 100kA, the fundamental and higher ECR layers (up to five resonances) coexist within the EXL-50's vacuum region within the limiters (as shown in Fig.1a). The electron density is measured by single-chord tangential microwave interferometer [27]. Two CdTe detectors with energy resolution are applied to observe the forward and backward bremsstrahlung hard x-ray (HXR) emission [28].

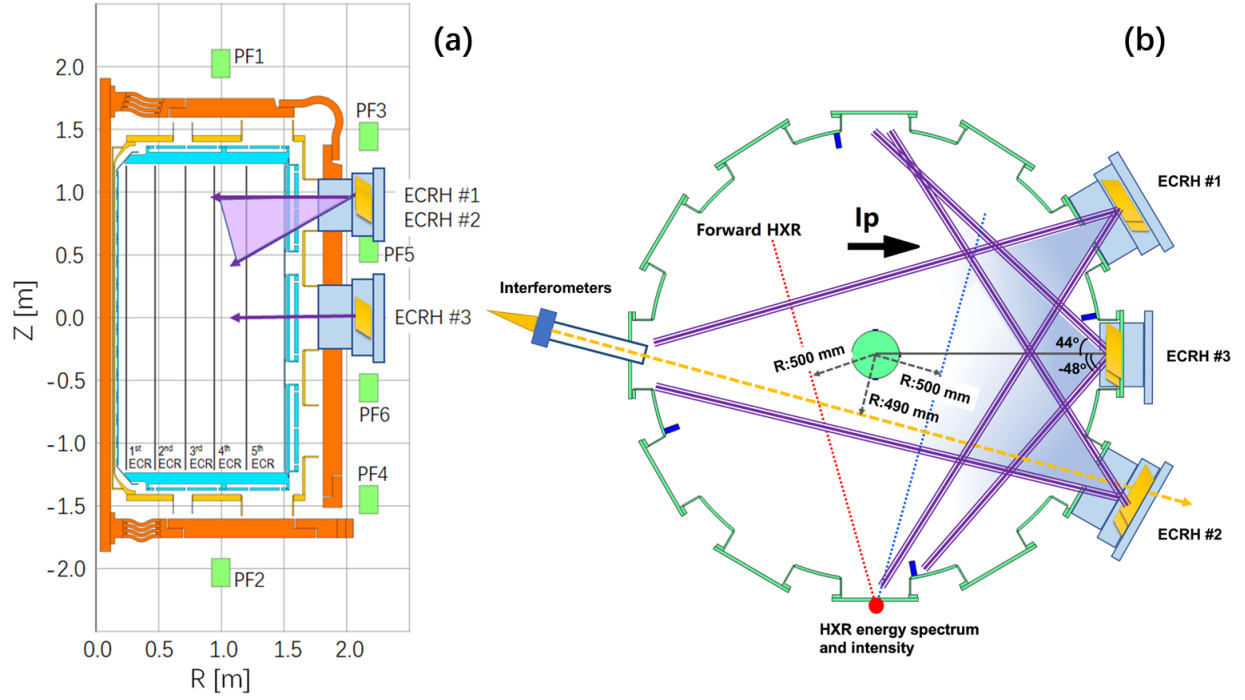


Fig.1 (a) Poloidal cross section of the EXL-50 device. Nominal toroidal field is 1 T at  $R = 0.24\text{m}$ . (b) Top view of EXL-50. The lines of sight of interferometer and HX diagnostics are indicated in the figure. The ECRH beam is aimed at the center of the machine when the toroidal injection angles is  $0^\circ$ .

**High efficiency current drive experimental results.** Here, a simplified current drive effectiveness  $\eta_{A/W}$  is defined as follows and utilized:

$$\eta_{A/W} = I_P / P_{ECRH}$$

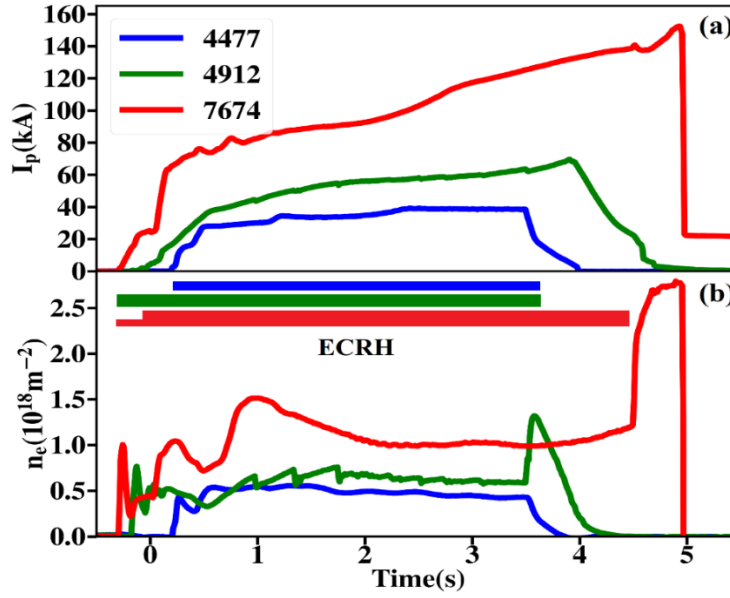


Fig.2 The discharge waveforms for different 28GHz ECRH heating power. (a) plasma current; (b) line integrated density. PECH was 20kW in shot 4477 and 45kW in shot 4912. Two gyrotrons are used in shot 7674. One gyrotron injected 20kW from -0.3s to 0s and the other gyrotron injected 115kW from 0s to 4.5s.

where  $I_p$  is the plasma current,  $P_{ECRH}$  is the ECRH power issued from the gyrotrons. Fig.2 shows the typical discharge waveforms with different 28GHz ECRH heating power in EXL-50. The  $\eta_{A/W}$  can reach 2A/W (40kA/20kW) for low power ECRH plasma. The  $\eta_{A/W}$  is 1.55A/W (70kA/45kW) for moderate power ECRH plasma and 1.22A/W (140kA/115kW) for further increased power ECRH plasma. The  $P_{ECRH}$  in this paper is the power measured at the matching optical unit (MOU) which is close to the exit power of the gyrotrons. The power delivered from the antenna inside the vacuum vessel is unknown at present. The duration of high current ( $I_p > 100\text{kA}$ ) for the higher power ECRH plasma in Fig.2 is more than 2s. The total pulse length for 28GHz ECR heating plasma is less than 6s limited by temperature rise at the top joints of the TF coils at 100kA electric current. One notable phenomenon as shown in Fig.2 is the density jumps as the ECRH power is turned off, indicating possibly a cessation of density pump-out by ECH [29] or confinement transition, which is not addressed in this paper.

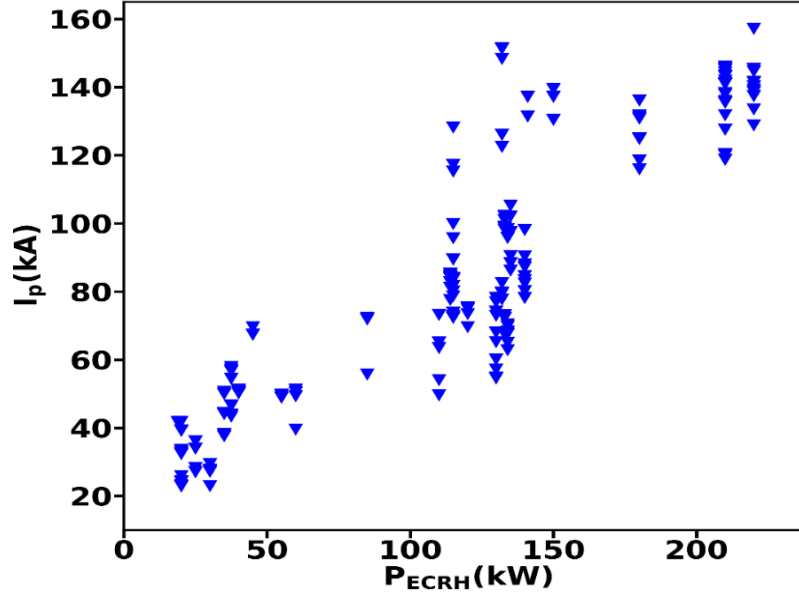


Fig.3  $I_p$  v.s.  $P_{ECRH}$  for 200 successful shots in EXL-50

Fig.3 shows the relation of  $I_p$  v.s.  $P_{ECRH}$  for about 200 successful shots in EXL-50. The general trend in Fig.3 is that the  $I_p$  increases with  $P_{ECRH}$ . On the other hand, it is also can be seen in Fig.3 that the  $I_p$  varies in quite large range for the same  $P_{ECRH}$ . The uncertainty of real injected and absorbed power by plasma may be one reason for the scattering relation between  $I_p$  and  $P_{ECRH}$  in Fig.3. At the same time, changes in the currents of PF coils and the vertical magnetic field  $B_v$  has substantial effects on  $\eta_{A/W}$ . For the same coil current,  $B_v$  (at  $R=0.5$  in middle plane) from PF56 is around 6 times as that of PF12 and 2 times as that of PF34. So, we design the special discharge experiments in fig.4a. In these shots, only PF56 is changed to show the effect of  $B_v$  on plasma current. The other parameters are same for these shots. Fig.4a clearly shows that the  $I_p$  increases with the current of PF5&6 coils for the same  $P_{ECRH}$  and density. The force balance between the expansion of the plasma itself and external magnetic compress must be sustained for a stable equilibrium structure. More statistical information from 200 shots is shown in Fig.4b. It can be found that the  $I_p$  increases with the external vertical magnetic field  $B_v$  in the appropriate  $P_{ECRH}$  range. Fig.4b also tell us that both  $B_v$  and  $P_{ECRH}$  are essential elements to increase the plasma current.  $B_v$  is not a plasma current driving source, but it will affect the maximum plasma current which is driven by ECRH. So much potential for raising  $\eta_{A/W}$  further remains unexplored at present through optimization and matching of PF coil current and power of ECRH, which will be explored and improved in future's experiment in EXL-50.

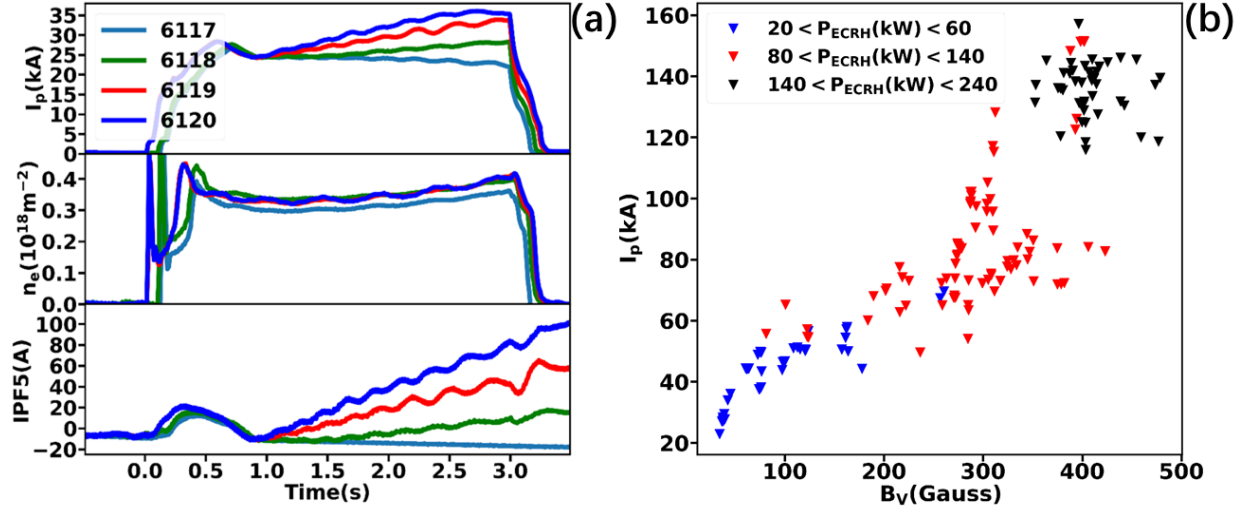


Fig.4 (a) The waveforms of four discharges with similar density. The waveforms from top to bottom are: plasma current; line integrated density; The electrical current of PF5.  $P_{\text{ECRH}}$  was 25kW for these shots. The electrical current of PF1 and PF3 were kept constant ( $I_{\text{PF1}}=100\text{A}$  and  $I_{\text{PF3}}=600\text{A}$ ) during whole discharge phase. (b) The plasma current at flat-top phase versus external  $B_v$  at  $R=0.5\text{m}$  in middle plane.

**Energetic electrons and current drive mechanisms.** The Pfirsch-Schluter (PS) current is a dominant component during the initial start-up phase, and drastically decreases with increasing  $B_v$  following the formation of CFS. The boot-strap current drive by the pressure gradient is at present estimated to be less than several percent for these EXL-50 plasmas. The conventional Electron cyclotron current drive (ECCD) via Fisch-Boozer mechanism [30] or Ohkawa mechanism [31] can also contribute to the non-inductive current. However, such ECCD effects which is sensitive to the ECRH injection angle have not been confirmed in EXL-50's experiments. Fig.5 shows the waveforms of two shots with same  $P_{\text{ECRH}}$  in EXL-50. Although the toroidal angle for the ECRH antenna was set at  $-16^\circ$  for count-current drive in shot 7448 and  $17^\circ$  for co-current drive in shot 7449, the plasma current remained largely unchanged. The single pass absorption of electron cyclotron wave (ECW) is very weak in the low temperature plasmas in current EXL-50 experiments. The angle and mode of ECW are changed during the multiple wall reflections, indicating that the conventional ECCD contribute to a negligible fraction of the total plasma current.

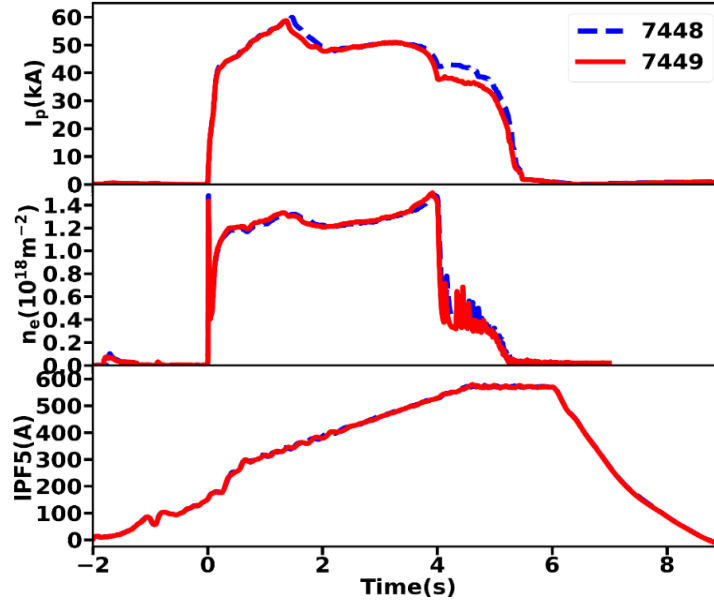


Fig.5 The waveforms of identical discharges with same density, ECRH power and PF current. (a) plasma current; (b) The electrical current of PF5; (b) line integrated density;

QUEST and LATE's experiments have proven that the energetic electrons play a primary role for the CS-free current drive. EXL-50's experimental results confirm that the plasma current is mainly carried by such energetic electrons. The shot shown in Fig.6 is a very stable and well-controlled discharge, showing a nearly stationary plasma current, electron density, as well as a zero loop voltage from 1.5s to 4.5s. During the entire discharge, the plasma current, and hard x-ray intensity and its photon temperature (the average energy of energetic electrons) vary conjointly in magnitude. It is seen that both the number and the energy of energetic electrons contribute directly to the increase of ECRH plasma current.

It should be noted that the role of induction in the CS-free ECRH driven current remains unresolved. That is, does the toroidal electric field induced by changes in the PF coil and plasma currents accelerate the already decoupled energetic electrons to even higher energies and carry a significant plasma current fraction during a discharge? Experiments dedicated to resolving this question were carried out. As indicated in Fig. 6a, the currents of PF3 and PF4 (not indicated) were kept constant during the entire discharge. The currents of PF1&2 and PF5&6 were ramped-up slowly until 1.5s and kept constant through to 6s. The loop voltage oscillated near zero between 1.5s and 2.5s and became zero between 2.5s and 4.5s. The loop voltage is main source to drive inductive plasma current. The largest value of loop voltage of +0.17V (counter-clockwise when



viewed from top) appears at 0.037s, in the direction opposite to the plasma current (clockwise when viewed from top). Therefore, the contribution to the inductive plasma current from loop voltage has negligible or negative contribution for the total plasma current during start-up and flattop phase.

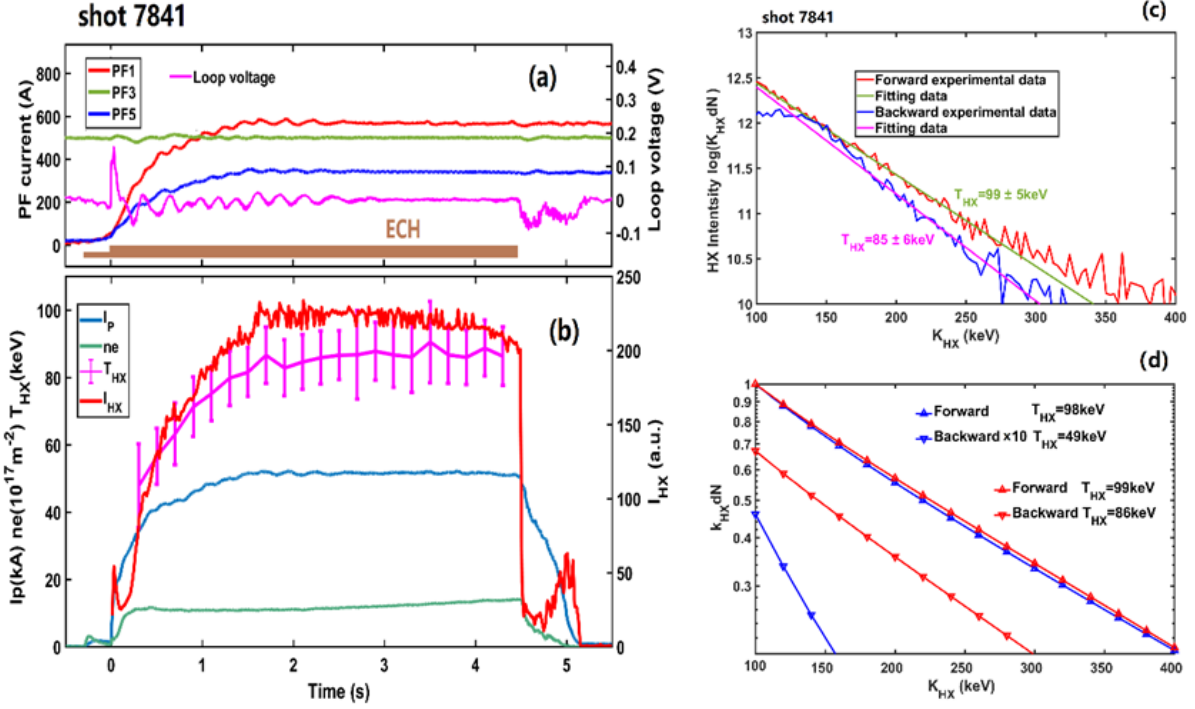


Fig.6 (a) Waveforms of PF current (PF1, PF3, and PF5), loop voltage and ECRH. (b) waveforms of plasma current ( $I_p$ ), density ( $n_e$ ), temperature ( $T_{HX}$ ) and intensity ( $I_{HX}$ ) of hard x-ray. One gyrotron injected 10kW from -0.3s to 0s and the other gyrotron injected 100kW from 0s to 4.5s. (c) HX spectrum (integrated time: 2s~2.2s) in forward and backward direction during flattop phase. (d) Simulated HX spectrum with three-temperature distribution model for energetic electron. Blue line:  $T_{//F}=10T_{\perp}=10T_{//B}$ . The backward data is magnified 10 times. The data is normalized with intensity at 100keV of forward HX. Red line:  $T_{//F}=T_{\perp}$ ,  $T_{//B}=0.75T_{//F}$ . The data is normalized with intensity at 100keV of forward HX.

In addition, the velocity distribution of energetic electrons driven by ECRH is different from that of runaway electrons induced by a toroidal electric field. In the former case, the energetic electrons possess similar magnitudes of parallel and perpendicular velocities, while in the latter, the parallel velocities dominate. Fig.6c shows the hard x-ray intensity and energy spectrum in forward (count-current) direction and backward (co-current) direction, indicating relatively moderate differences. The three-temperature Maxwellian distribution model (3T model) [32, 33] can be applied for the anisotropic distribution of runaway electrons or energetic electrons in RF heating plasmas. The simulated HX spectrum based on 3T model is shown in Fig.6d. For the runaway distribution case

(blue line in Fig.6d), the simulated backward HX intensity at 100keV is less than 1/20 as that of forward HX intensity. The photon temperature of HX of backward is only half as that of forward in runaway cases. Compared to the runaway simulation cases, the simulated HX spectrum based on the distribution of equal parallel forward and perpendicular temperature (red line in Fig.6d) is much more approximate to the experimental data in Fig.6c. On the other hand, the energetic electrons can be strongly accelerated in the parallel direction by the relative high loop voltage during current ramp-down after the ECRH is turned off. These experimental observations indicate that the inductive and runaway-like current drive mechanisms are not significant in the CS-free ECRH plasmas.

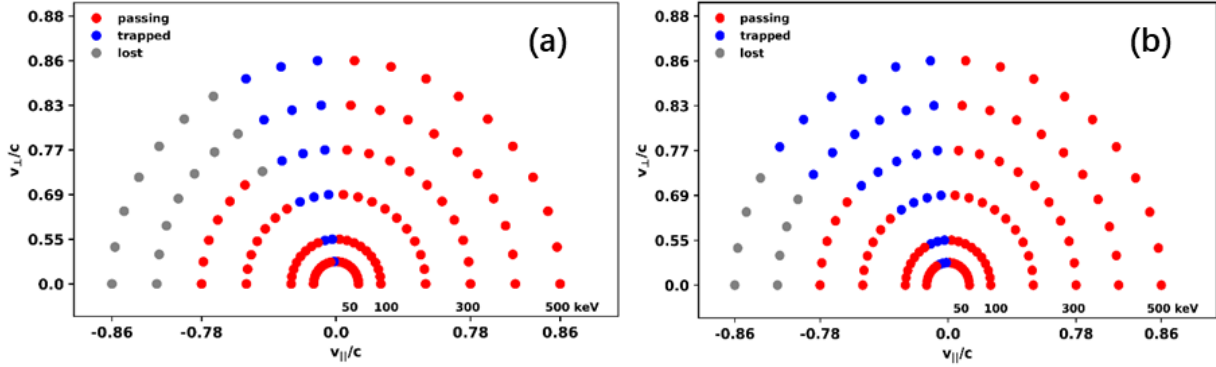


Fig.7 (a) Velocity distribution of energetic electrons which start from 1st harmonica layer at mid-plane. (b) Velocity distribution of energetic electrons which start from magnetic axis.

A key question regarding the very high current drive effectiveness ( $\eta_{A/W} = 1.2 \sim 2$  A/W) in EXL-50 via the energetic electrons may be addressed by analysing the asymmetric region of orbit containment of the energetic electrons. Fig.7 shows the orbit confinement analysis for energetic electrons in velocity-energy space. A three-fluid equilibrium reproducing a 50kA EXL-50's plasma was obtained via the multi-fluid equilibrium model [33] for the computation for the guiding-center orbits [34]. A strongly asymmetric distribution in the parallel direction of the contained orbits in the  $v_{\parallel}$ ,  $v_{\perp}$ , and energy space, is obtained, accentuated as the electron energy increases toward the limiting energy of orbit containment. The asymmetric structure of the contained energetic electron orbits as shown in fig.7 is determined by the PF coil currents, not by the ECRH injected angle. The population of energetic electrons is mainly related to the density and power of ECRH. As mentioned above, the conventional ECCD mechanisms produce a minor contribution to the total plasma current in EXL-50. Although the ECRH injection angles are quite

different in the shots in fig.5, the plasma currents are quite similar because the other main parameters such as the PF setting, density and ECRH power are same. Further, the design of EXL-50 (as shown in Fig.1a) permits the coexistence of five ECR layers within the vacuum vessel. Considering the effect of relativistic Doppler shift [23], the resonance layers for energetic electrons broaden in major radius. Fig.8a shows the radial dependence of the characteristic resonant energies for the fundamental and harmonic ECW for EXL-50. For energy of electrons above 100keV, the width of a resonance upshifts to overlap with the downshifted resonance of the next higher harmonic. It can be seen that the individual resonance widths for the energetic electrons fill the entire space inside EXL-50's vacuum vessel.

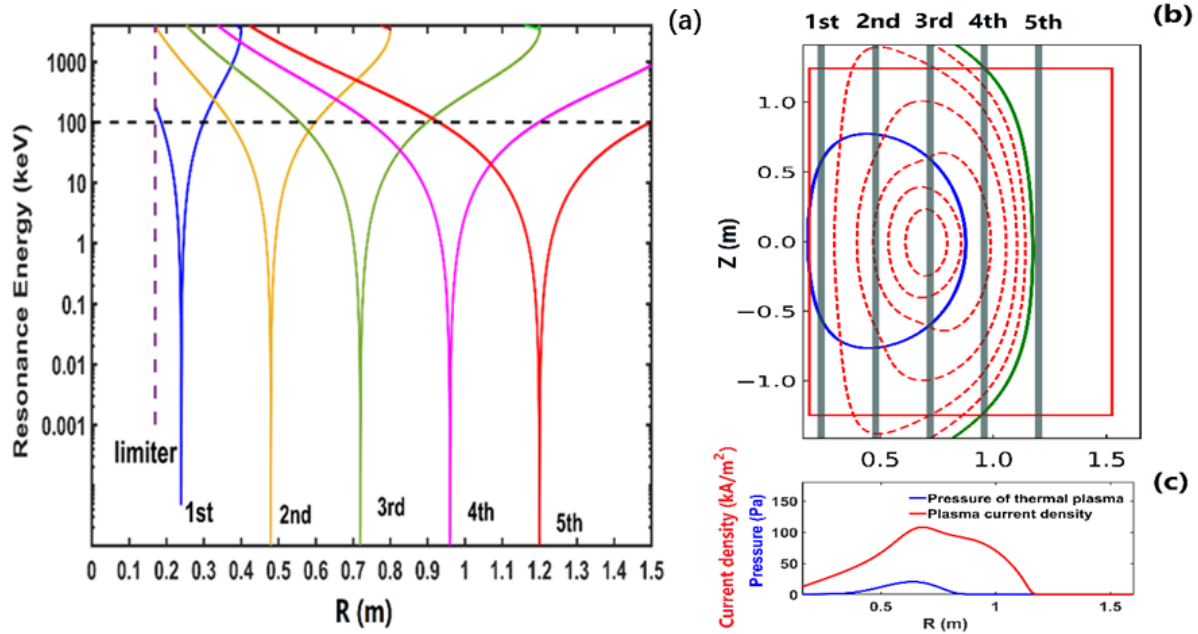


Fig.8 (a) Radial profiles of resonance energy for the harmonic ECW. (b) Reconstructed 2D contour plot of plasma current by the multi-fluid equilibrium model. Blue line represents LCFS. (c) The radial profiles of thermal plasma pressure and current density

The single-pass absorption of ECW is estimated to be relatively low in EXL-50 for the present range of plasma densities and temperatures. The smooth stainless steel vacuum vessel walls and limiters, including those on the center column, assist in ensuring multiple reflected paths of the injected ECW back to the plasma. Wall-reflection further helps by converting O-mode wave to the X-mode and vice versa, thus taking advantage of the higher efficiency of X-modes by energetic electrons [26]. Another notable feature of EXL-50's plasma is that the cross section of the plasma current carried by the energetic electrons is much bigger than that of CFS during the flattop phase

of plasma current. Fig.8b and c show 2D contour plot of plasma current, last close flux surface (LCFS), and the profiles of thermal plasma and current for a 120kA discharge shown in Fig.2, computed via the multi-fluid equilibrium model [30]. A significant fraction of the plasma current (52% in this case) is flowing outside the LCFS. The phenomenon that the energetic electrons play a substantial role in the formation of closed flux surface and carry a dominant fraction of the plasma current that extends over the open field region in the solenoid-free ECRH sustained ST plasmas have been confirmed in LATE [11,12]. Similar analysis has been also conducted in EXL-50. As a first approximation, a multi-fluid equilibrium model that includes a high-energy electron component in addition to a low-energy electron and ion components was applied to describe the equilibrium characteristics of EXL-50. The simulation results were matched well to the available experimental data [33].

**High density current drive experiment.** High density ECRH discharges are also obtained in EXL-50. The line averaged density can be as higher as three times of the ordinary mode (O-mode) cut-off density in the 2.45GHz ECH discharges. In the 28GHz ECH discharges, the line average density near the O-mode cut-off ( $\sim 9 \times 10^{18} \text{m}^{-3}$ ) has been measured. The core density for shot 7814 in Fig.9 would exceed the cut-off density if the density profile within the LCFS has a parabolic shape. It is surmised that the electron Bernstein wave (EBW) has been excited and played key role to heat plasma and drive current for such high density discharges. In shot 7814, density ramp-up caused a decrease in plasma current. In fact, the continuous current decrease during the density flattop is mainly caused by the yet-to-be optimized PF current setting. After eliminating the influence of PF current, the plasma current only decrease one third (from 116kA to 76kA) when the line density increases 6 times (from  $0.11 \times 10^{19}$  to  $0.77 \times 10^{19} \text{m}^{-2}$ ). The hard x-ray signal in Fig.9 indicates that the energetic electron can be still efficiently produced and maintain a dominant component of the plasma current in high density ECH discharges.

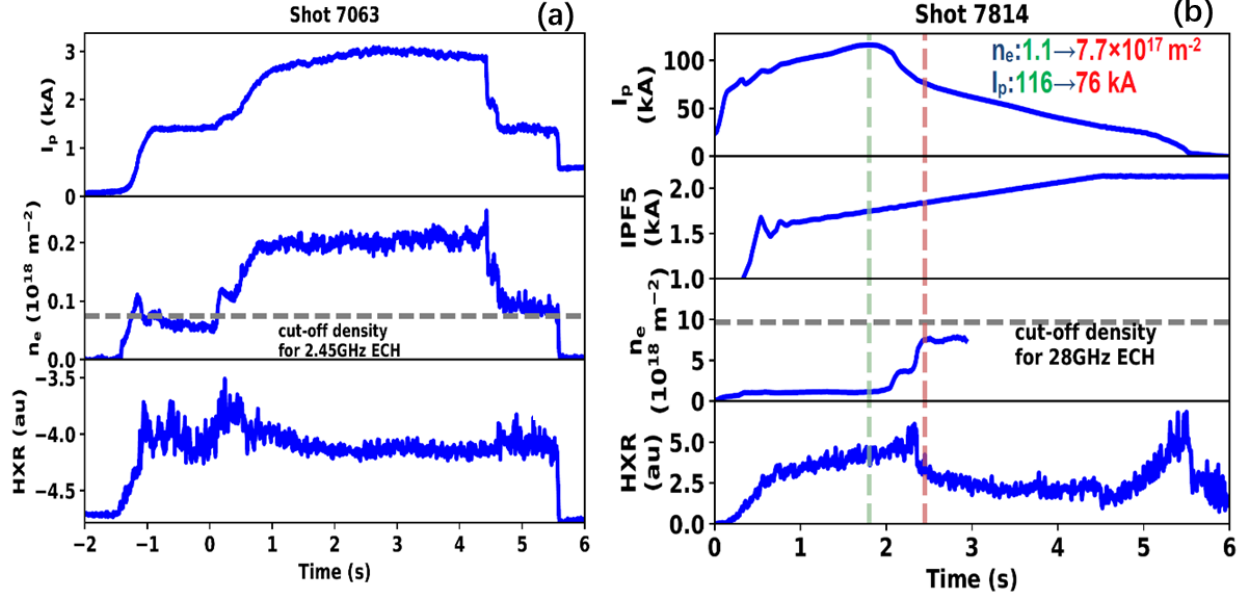


Fig.9 (a) Waveforms of high density discharge with 2.45GHz ECRH. PECRH was 20kW. The waveforms from top to bottom are plasma current,  $I_p$ ; line integrated density; intensity of hard x-ray. (b) Waveforms of high density discharge with 28GHz ECRH. PECRH was about 200kW. The waveforms from top to bottom are plasma current  $I_p$ ; electrical current of PF5; line integrated density; intensity of hard x-ray.

**Summary** New records of driven plasma current and current drive effectiveness have been obtained during the CS-free ECRH-only operation on EXL-50. The energetic electrons play a unique and important role in EXL-50's plasmas. Metal wall of the vacuum vessel effecting multi-reflective absorption of high multi-harmonic resonances resulted in highly effective acceleration of the energetic electrons. The asymmetric distribution of the energetic electrons in velocity-energy space based on orbit analysis in a multi-fluid equilibrium is another key feature of the very high current driven effectiveness observed. However, the physics mechanism for the solenoid-free ECRH current drive is not yet well understood and quantifiable. Nevertheless, these results demonstrate an exceptional potential of ECRH to achieve and maintain highly efficient steady-state current drive under low and high densities in the CS-free EXL-50 device. Theory, modelling and simulation to better describe the full range of mechanisms associated with the CS-free current drive observed will be systematically developed in the future. Steady-state high current and density experiments using high ECRH power on EXL-50 will continue to make additional physics contributions towards an eventual realization of a commercial fusion reactor.

## Methods

### Simulation of hard x-ray spectrum based on three-temperature distribution model for energetic electrons

The anisotropic velocity distribution function  $f_s$  of the suprathermal electrons in magnetic confined plasma can be represented by a three-temperature Maxwellian model (3T model) [32].

$$f_s(\vec{p}) = C_N \exp\left(-\frac{p_\perp^2}{2T_\perp} - \frac{p_\parallel^2}{2T_{\parallel F}}\right) \text{ for } p_\parallel \geq 0$$

$$f_s(\vec{p}) = C_N \exp\left(-\frac{p_\perp^2}{2T_\perp} - \frac{p_\parallel^2}{2T_{\parallel B}}\right) \text{ for } p_\parallel < 0$$

$$\text{and } f_s(\vec{p}) = 0, \text{ for } \vec{p} > p_c$$

where  $p_\parallel$  and  $p_\perp$  are the parallel and perpendicular components of the momentum with respect to the magnetic field, normalized to the electron rest momentum  $m_e c$ ;  $T_\perp$ ,  $T_{\parallel F}$  and  $T_{\parallel B}$  are the perpendicular, parallel forward and parallel backward temperature, respectively, normalized to the electron rest mass  $m_e c^2$ ;  $p_c$  is the upper cut-off momentum ( $p_c = \sqrt{(10T_{\parallel F} + 1)^2 - 1}$  in simulation). For the runaway electrons, the perpendicular and parallel backward velocities are much smaller than the parallel forward velocity. So,  $T_{\parallel F} \gg T_\perp$  and  $T_{\parallel B}$  in 3T model can represent the distribution of runaway electrons. For the energetic electrons generated by RF heating, the perpendicular and parallel backward velocities are same order as the parallel forward velocity.  $T_{\parallel F} \sim T_\perp$  and  $T_{\parallel B}$  in 3T model is a good approximation for the distribution of energetic electrons in RF plasma.

Only the electron-ion bremsstrahlung radiation is considered for the hard x-ray simulation. The electron-electron bremsstrahlung and recombination radiation can be neglected compare to the electron-ion bremsstrahlung [32]. The x-ray is the line integrated measurement. The radial profile of ion density, energetic electron density and temperatures in 3T model are the key parameters to determine the shape of HX spectrum. For the simulation of HX spectrum in EXL-50, the energetic electron density is assumed as constant in thermal plasma region. The profiles of the ion density and energetic electron temperatures are assumed as parabolic distribution.  $T_\perp / T_{\parallel F}$  and  $T_{\parallel B} / T_{\parallel F}$  are 0.1 and 0.1 for runaway case, 1 and 0.75 and for ECRH case, respectively. The ratio of  $T_\perp / T_{\parallel F}$

and  $T_{||B} / T_{||F}$  is fixed and not change with radius. Under the above assumption, the best fitting of forward HX spectrum for 7841 in Fig.6 can be obtained when the peak value of  $T_{||F}$  is setting as 580keV for runaway case and 420keV for ECRH case.

## Reference

- [1] Artsimovich, L. A., Brobrovskii, G. A., Gorbunov, E. P., Ivanov, D. P., Kirillov, V. D., Kuznetsov, E. I., Mirnov, S. V., Petrov, M. P., Rasumova, K. A., Strelkov, V. S., and Shcheglov, D. A., Proc. Third Intern. Conf. on Plasma Physics and Nuclear Fusion, Novosibirsk, 1968, 1, 157 (Paper CN24/B1) (International Atomic Energy Agency, Vienna, 1969)
- Artsimovich, L. A. et al., Thermal insulation of plasma in the Tokamaks, 1967 Sov. At. Energy (Soviet Atomic Energy) 22 325-331
- [2] N. J. Peacock, D. C. Robinson, M. J. Forrest, P. D. Wilcock & V. V. Sannikov, Measurement of the Electron Temperature by Thomson Scattering in Tokamak T3, Nature 224, 488 - 490 (01 November 1969); doi:10.1038/224488a0
- [3] Peng Y.-K.M. and Strickler D.J., Features of spherical torus plasmas, Nucl. Fusion 26 769-777 (1986)
- [4] Peng Y.-K.M., The physics of spherical torus plasmas, Phys. Plasmas 7, 1681-1692 (2000).
- [5] Sykes A., Akers R., Appel L., Carolan P.G., Conway N.J., et al, High- performance of the START spherical tokamak , Plasma Phys. Control. Fusion 39, B247-260(1997)
- [6] Synakowski E.J., Bell M. G., Bell R.E., Bigelow T., Bitter M., et al., The national spherical torus experiment (NSTX) research programme and progress towards high beta, long pulse operating scenarios, Nucl. Fusion 43 1653-1664 (2003)
- [7] Buttery R. J., Akers R., Arends E., Conway N. J., Counsell G. F., et al., Stability at high performance in the MAST spherical tokamak, Nucl. Fusion 44 1027-1035 (2004)
- [8] V.K. Gusev, S.E. Aleksandrov, V. Kh Alimov, I.I. Arkhipov, B.B. Ayushin, et al., Overview of results obtained at th Globus-M spherical tokamak, Nucl. Fusion 49 104021 (2009)
- [9] Y.-K. M. Peng et al, Introduction to the ENN XuanLong (EXL) Innovation and Research, to be submitted.
- [10] C. B. Forest, Y. S. Hwang, M. Ono, and D. S. Darrow, Internally Generated Currents in a Small-Aspect-Ratio Tokamak Geometry, Phys. Rev. Lett. 68, 3559-3562 (1992)

- [11] T. Maekawa, Y. Terumichi, H. Tanaka, M. Uchida, T. Yoshinaga, Formation of spherical tokamak equilibria by ECH in the LATE device, *Nucl. Fusion* 45 1439-1445 (2005)
- [12] T. Yoshinaga, M. Uchida, H. Tanaka, and T. Maekawa, Spontaneous Formation of Closed-Field Torus Equilibrium via Current Jump Observed in an Electron-Cyclotron-Heated Plasma, *Phys. Rev. Lett.* 96, 125005 (2006)
- [13] M. Uchida, T. Yoshinaga, H. Tanaka, T. Maekawa, Rapid Current Ramp-Up by Cyclotron-Driving Electrons beyond Runaway Velocity, *Phys. Rev. Lett.* 104, 065001 (2010)
- [14] K. Kuroda, M. Wada, M. Uchida, H. Tanaka, T. Maekawa, Shift in principal equilibrium current from a vertical to a toroidal one towards the initiation of a closed flux surface in ECR plasmas in the LATE device, *Plasma Phys. Control. Fusion* 58, 025013 (2016)
- [15] H. Tanaka, Y. Nozawa, M. Uchida, R. Kajita, Y. Omura, et al., Electron Bernstein wave heating and current drive with multi-electron cyclotron resonances during non-inductive start-up on LATE, in *Proceedings of 27th IAEA Fusion Energy Conference, Ahmedabad, India (2018)*, p. EX/P3-19
- [16] A. Ejiri, Y. Takase, T. Oosako, T. Yamaguchi, Y. Adachi, et al., Non-inductive plasma current start-up by EC and RF power in the TST-2 spherical tokamak, *Nucl. Fusion* 49 065010 (2009)
- [17] Y. Takase, A. Ejiri, H. Kakuda, T. Oosako, T. Shinya, Non-inductive plasma initiation and plasma current ramp-up on the TST-2 spherical tokamak, *Nucl. Fusion* 53 063006 (2013)
- [18] V.F. Shevchenko, M.R. O'Brien, D. Taylor, A.N. Saveliev, Electron Bernstein wave assisted plasma current start-up in MAST, *Nucl. Fusion* 50 022004 (2010)
- [19] V. F. Shevchenko, T. Bigelow, J. B. Caughman, S. Diem, J. Mailloux, et al., Long Pulse EBW start-up experiments in MAST, *EPJ Web Conf.* 87, 02007 (2015)
- [20] K. Hanada, H. Zushi, H. Idei, K. Nakamura, M. Ishiguro, et al., Non-Inductive Start up of QUEST Plasma by RF Power, *Plasma Science and Technology*, 13, 307-311 (2011)
- [21] M. Ishiguro, K. Hanada, H. Liu, H. Zushi, K. Nakamura, et al., Non-inductive current start-up assisted by energetic electrons in Q-shu University experiment with steady-state spherical tokamak, *Phys. Plasmas* 19, 062508 (2012)
- [22] S. Tashima, H. Zushi, M. Isobe, K. Hanada, H. Idei, et al., Role of energetic electrons during current ramp-up and production of high poloidal beta plasma in non-inductive current drive on QUEST, *Nucl. Fusion* 54, 023010 (2014)



- [23] H. Idei, T. Kariya, T. Imai, K. Mishra, T. Onchi, et al., Fully non-inductive second harmonic electron cyclotron plasma ramp-up in the QUEST spherical tokamak, Nucl. Fusion 57,126045 (2017).
- [24] H. Idei, T. Onchi, T. Kariya, et al., fully non-inductive 2nd harmonic electron cyclotron current ramp-up with polarized focusing-beam in the quest spherical tokamak, in Proceedings of 27th IAEA Fusion Energy Conference, Ahmedabad, India (2018), EX/P3-21
- [25] H. Idei, T. Onchi, K. Mishra, H. Zushi, T. Kariya, et al., Electron heating of over-dense plasma with dual-frequency electron cyclotron waves in fully non-inductive plasma ramp-up on the QUEST spherical tokamak, Nucl. Fusion 60, 016030 (2020)
- [26] T. Onchi, H. Idei, M. Fukuyama, D. Ogata, R. Ashida, et al., Non-inductive plasma current ramp-up through oblique injection of harmonic electron cyclotron waves on the QUEST spherical tokamak, Phys. Plasmas 28, 022505 (2021)
- [27] S.J. Li, R.H. Bai, R.Y. Tao, N. Li, X.C. Lun, L.C. Liu, Y. Liu, M.S. Liu and B.H. Deng, A quasi-optical microwave interferometer for the XuanLong-50 experiment, Journal of Instrum. 16, T08011(2021)
- [28] S. K. Cheng, Y. B. Zhu, Z. Y. Chen, Y. X. Li, R. H. Bai, B. Chen, X. L. Huang, L. L. Dai, and M. S. Liu, Tangential hard x-ray diagnostic array on the EXL-50 spherical tokamak, Rev. Sci. Instrum. 92, 043513 (2021)
- [29] C. Angioni, E. Fable, M. Greenwald, M. Maslov, A. G. Peeters, H. Takenaga and H. Weisen, Particle transport in tokamak plasmas, theory and experiment, Plasma Phys. Control. Fusion 51, 124017 (2009)
- [30] N.J.Fisch, and A.H. Boozer, Creating an Asymmetric Plasma Resistivity with Waves, Phys. Rev. Lett. 45, 720-722 (1980)
- [31] T. Ohkawa, Steady-state operation of tokamaks by r-f heating, General Atomics Report No. GA-A13847 (1976).
- [32] J.Stevens, S. Von Goeler, S. Bernabei, M. Bitter, T.K.Chu, et al., Modelling of the electron distribution based on bremsstrahlung emission during lower-hybrid current drive on PLT, Nucl. Fusion 29, 1529-1541 (1985)
- [33] A. Ishida, Y.K. M. Peng, W. J. Liu, Four-Fluid Axisymmetric Plasma Equilibrium Model Including Relativistic Electrons and Computational Method and Results, Phys. Plasmas 28, 032503 (2021)
- [34] T. Maekawa, T. Yoshinaga, M. Uchida, F. Watanab and H. Tanaka, Open field equilibrium current and cross-field passing electrons as an initiator of a closed flux surface in EC-heated toroidal plasmas, Nucl. Fusion 52, 083008 (2012)

y.